EXPERIMENTAL AND NUMERICAL ANALYSIS OF RC TWO-SPAN SLABS STRENGTHENED WITH NSM CFRP LAMINATES

By Dalfré[1], G. and Barros[2], J.A.O.

Synopsis: This work reports the results of an ongoing research program on the use of the near surface mounted (NSM) CFRP laminates for the flexural strengthening of continuous reinforced concrete (RC) slabs. The experimental program is formed by two slab strips of two equal span lengths, and has the main purpose of verifying the possibility of increasing the negative resisting bending moment in 25%, maintaining a relatively high level of moment redistribution. To assess the predictive performance of a FEM-base computer program, the experimental results are compared with the values estimated by the numerical analysis carried out using a FEM-based computer program. The results show that the proposed strengthening technique is able to increase significantly the load carrying capacity of RC slabs. However, the load carrying capacity of the strengthened slabs was limited by the detachment of the strengthened concrete cover layer at the intermediate support. The numerical model predicts with high accuracy the behavior of this type of structures.

KEYWORDS: CFRP, Continuous RC slabs strips, Flexural strengthening, NSM, Moment redistribution

Gláucia Dalfré is a PhD Student of ISISE, Department of Civil Engineering, University of Minho, Portugal. She received her MSc from São Carlos School of Engineering, University of São Paulo, Brazil. Her research interests include structural analysis and modeling; fiber-reinforced composites, including repair and retrofit of civil infrastructures.

Joaquim Barros is an Associate Professor and Director of the Laboratory of the Structural Group of the Department of Civil Engineering, University of Minho. He received his MSc and PhD from the University of Porto, Portugal. He is a member of ACI Committees 440 and 544, and fib TG 8.3 and 9.3. His research interests include structural strengthening, composite materials, fiber reinforced concrete and finite element method.

INTRODUCTION

In general, when a structural Reinforced Concrete (RC) element is strengthened with fiber reinforced polymer (FRP) systems, its failure mode tends to be more brittle than its unstrengthened homologous element, due to the intrinsic bond conditions between these systems and the concrete substrata, as well as the linear-elastic brittle tensile behavior of FRPs. In case of continuous RC slabs and beams (statically indeterminate structures), the use of FRP systems to increase their flexural resistance can even compromise the moment redistribution capacity of these types of elements.

Externally Bonded Reinforcement, EBR (ACI 440 2007, FIB 2001), and the Near Surface Mounted, NSM (Barros and Kotynia 2008; Barros *et al.* 2007) are the most used techniques for the strengthening of RC elements. However, when compared to EBR, the NSM technique is especially appropriate to increase the negative bending moments (in the intermediate supports) of continuous RC slabs since its strengthening process is simpler and faster to apply than other FRP-based techniques (Barros and Kotynia 2008). The efficiency of the NSM technique for the flexural (Barros and Fortes 2005; De Lorenzis *et al.* 2000; Carolin 2003; El-Hacha and Rizkalla 2004; Liu *et al.* 2006; Nordin 2003) and shear (Barros and Dias 2006, Dias and Barros 2008, Dias and Barros 2010; Anwarul Islam 2009) strengthening of RC members has already been assessed. However, most of the tests were carried out with simply supported NSM strengthened members.

Although many in situ RC elements are of continuous construction, there is a lack of experimental and theoretical studies in the behavior of statically indeterminate RC members strengthened with FRP materials. Related to the analysis of the behavior of continuous elements, the majority of research studies reports the use of EBR technique (El-Refaie *et al.* 2003; Ashour *et al.* 2004; Grace *et al.* 2004; Akbarzadeh Bengar and Maghsoudi 2009, Vasseur 2009). Limited information is available in literature dealing with the behavior of continuous structures strengthened according to the NSM technique (Liu 2005; Liu *et al.* 2006; Bonaldo 2008). In the present paper the potentialities of the NSM technique is explored for the increase of the load carrying capacity of two spans continuous RC slabs. The NSM strengthening configurations applied in the slab strip were designed to increase in 25% the load carrying capacity of its corresponding unstrengthened control RC slab. Besides the load carrying capacity of the tested slabs, the moment redistribution issue is discussed in this paper.

EXPERIMENTAL PROGRAM

Specimen and Test Configuration

The experimental program is composed by the two RC slab strips with the geometry, support and load conditions, reinforcement and strengthening arrangements represented in Figure 1. The steel reinforcement arrangements in the reference slab (with the designation of SL30) were designed for a load of 46.2 kN (10.4 kips), which is the load that introduces a deflection of L/480 (L=2800 mm [110.24 in.] is the span length of the slab) recommended by the ACI 318 (2004), and assuming a moment redistribution of 30%. Furthermore, in the evaluation of these reinforcement arrangements a strain limit of 3.5‰ for the concrete crushing was assumed.
According to the CEB-FIB Model Code (1993), the coefficient of moment redistribution, $\delta = M_{red}/M_{elas}$, is defined as the relationship between the moment in the critical section after redistribution (M_{red}) and the elastic moment (M_{elas}) in the same section calculated according to the theory of elasticity, while $\eta = (1-\delta)\cdot 100$ is the moment redistribution percentage. The NSM flexural strengthened slab has the same steel reinforcement arrangement adopted in the reference slab, and a number of CFRP laminates applied in the hogging (intermediate support) and sagging regions (loaded zones) designed in order to increase the load carrying capacity of the reference slab (REF) in 25%.
The design of cross sections subject to flexure was based on stress and strain compatibility, where the maximum strain at extreme concrete compression fiber was assumed equal to 0.0035. In order to increase the load carrying capacity in 25% the strengthening arrangement represented in Figure 1 (c) was adopted. In the hogging region, two 1.4×20 mm^2 (0.05×0.79 in.^{2}) cross section area CFRP laminates were applied, while in both sagging regions two 1.4×20 mm^2 (0.05×0.79 in.^{2}) and two 1.4×10 mm^2 (0.05×0.39 in.^{2}) CFRP laminates were installed. This slab has the designation of SL30s25.
The test with the strengthened slab strip had two phases. In the first phase the slab was loaded up to attain in the loaded sections a deflection corresponding to 50% of the deflection measured in the reference slab when steel reinforcement in the hogging region (H) has attained its yield strain. When attained this deflection level (5.8 mm [0.23 in.]), a temporary reaction system was applied (Figure 2) in order to maintain this deformability during the period necessary to strengthen the slab. To control the maintenance of this deflection, dial gauges were used in order to adjust the temporary reaction system when necessary. Therefore, the strengthening process was applied maintaining the slab with a damage level that can be representative of real slabs requiring structural rehabilitation. After the curing time of the adhesives used to bond the NSM CFRP strips (which in general took about two weeks), the temporary reaction system was removed, while the load was transferred to the slab. This stress transfer process was governed by the criteria of maintaining the deflection level that corresponds to the initiation of the second phase of the test (5.8 mm [0.23 in.]). This second phase ended when the strengthened slab strip has ruptured.

Measuring Devices

Figure 3 depicts the positioning of the sensors for data acquisition in the tests. To measure the vertical deflection of a slab strip, six linear voltage differential transducers

(LVDT 82803, LVDT 60541, LVDT 82804, LVDT 19906, LVDT 18897 and LVDT 3468) were supported in a suspension bar (Figures 2 and 3a).

The LVDTs 60541 and 18897, placed at the slab loaded sections, were also used to control the test at a displacement rate of 10 μm/s up to the deflection of 50 mm (1.97 in.). After this deflection, the internal LVDTs of the actuators were used to control the test at a displacement rate of 20 μm/s up to the failure of the slab strip.

The force ($F_{(522)}$) applied at the left span (Figure 3a) was measured using a load cell of ±200 kN (44.9 kips) and accuracy of ±0.03% (designated Ctrl_1), placed between the loading steel frame and the actuator of 150 kN (33.7 kips) load capacity and 200 mm (7.9 in.) range. In the right span, the load ($F_{(123)}$) was applied with an actuator of 100 kN (22.5 kips) and 200 mm (7.9 in.) range, and the corresponding force was measured using a load cell of ±250 kN (56.2 kips) and accuracy of ±0.05% (designated Ctrl_2). To monitor the reaction forces, load cells were installed under two supports. One load cell (AEP_200) was positioned at the central support (nonadjustable support), placed between the reaction steel frame (HEB 300 profile) and the slab's support device (Fig. 3a). The other load cell (MIC_200) was positioned in-between the reaction steel frame and the apparatus of the adjustable right support of the slab. These cells have a load capacity of 200 kN (44.9 kips) and accuracy of ±0.05%.

To monitor the strain variation in the steel bars, concrete and CFRP laminates, the arrangements of strain gauges (SGs) represented in Figure 3(b-e) were adopted. Eleven SGs were installed in steel bars, seven of them in steel bars at top surface in the hogging region (SG1 to SG7) and the other four in steel bars at bottom surface in the sagging regions (SG8 to SG11, Figure 3b-c). Six SGs were applied at the external concrete surface in the compression regions (SG12 to SG17, Figure 3d). Finally, three SGs (SG18 to SG20) were bonded along one CFRP laminate in the hogging region and three SGs (SG21 to SG23 and SG24 to SG26) were installed along one CFRP laminate in both sagging regions (Figure 3e).

Material PropertieS

Tables 1 and 2 include values obtained from experimental tests for the characterization of the main properties of the materials used in the present work. The compressive strength and the static modulus of elasticity in compression were determined according to NP-E397 (1993). To characterize the steel bars, uniaxial tensile tests were conducted according to the standard procedures of ASTM 370 (2002). Unidirectional pultruded CFRP laminates, supplied by "S&P Clever Reinforcement Ibérica Company" were used in this study and their tensile behaviour was assessed by performing uniaxial tensile tests carried out according to ISO 527-1 (1993) and ISO 527-5 (1993) recommendations. Both CFRP laminates have a width of 1.4 mm (0.05 in.). For the characterization of the tensile behaviour of the epoxy adhesive, uniaxial tensile tests were performed complying with the procedures outlined in ISO 527-2. For the adhesive, an elasticity modulus and a tensile strength of 18.60 GPa (2697 ksi) [11.46%], and 21.12 MPa (3063 psi) [6.06%] were obtained, respectively, where the values between square brackets correspond to the coefficient of variation.

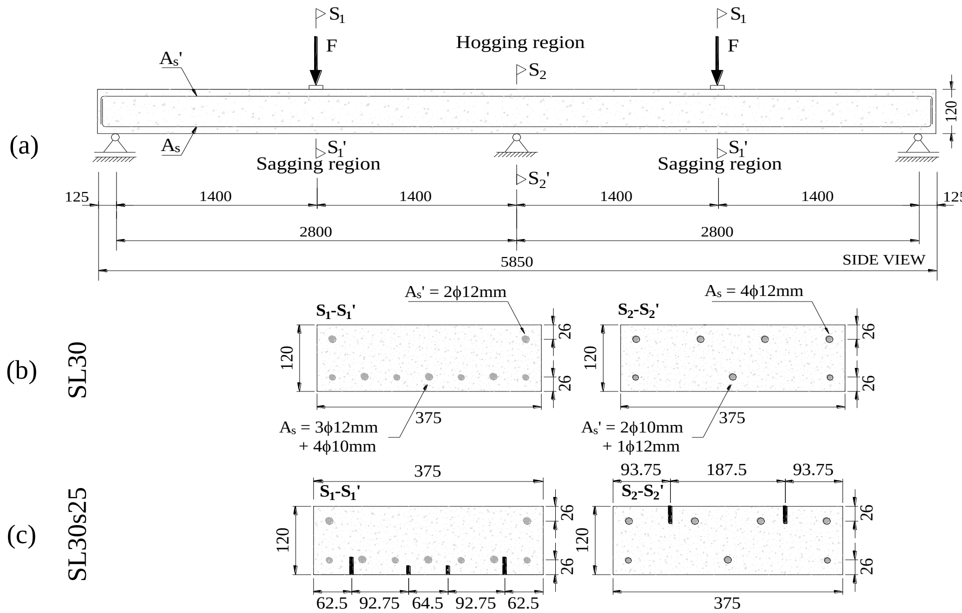

Figure 1 — Slab strips: (a) test configurations, (b and c) specimens cross-sectional dimensions of sagging (S1-S1') and hogging regions (S2-S2'). All dimensions are in mm (1 mm = 0.04 in.).

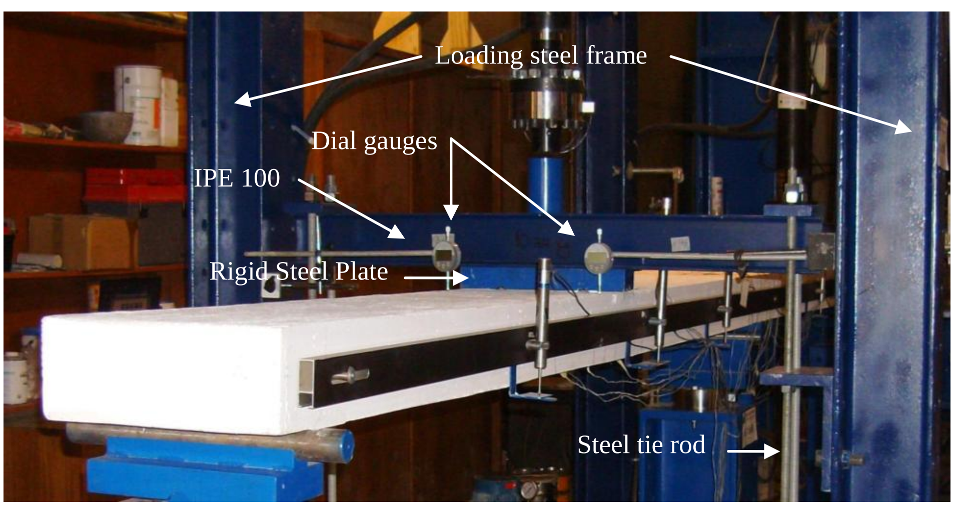

Figure 2 — Apparatus to sustain and control the mid-span displacement level applied in the slab strips to be strengthened.

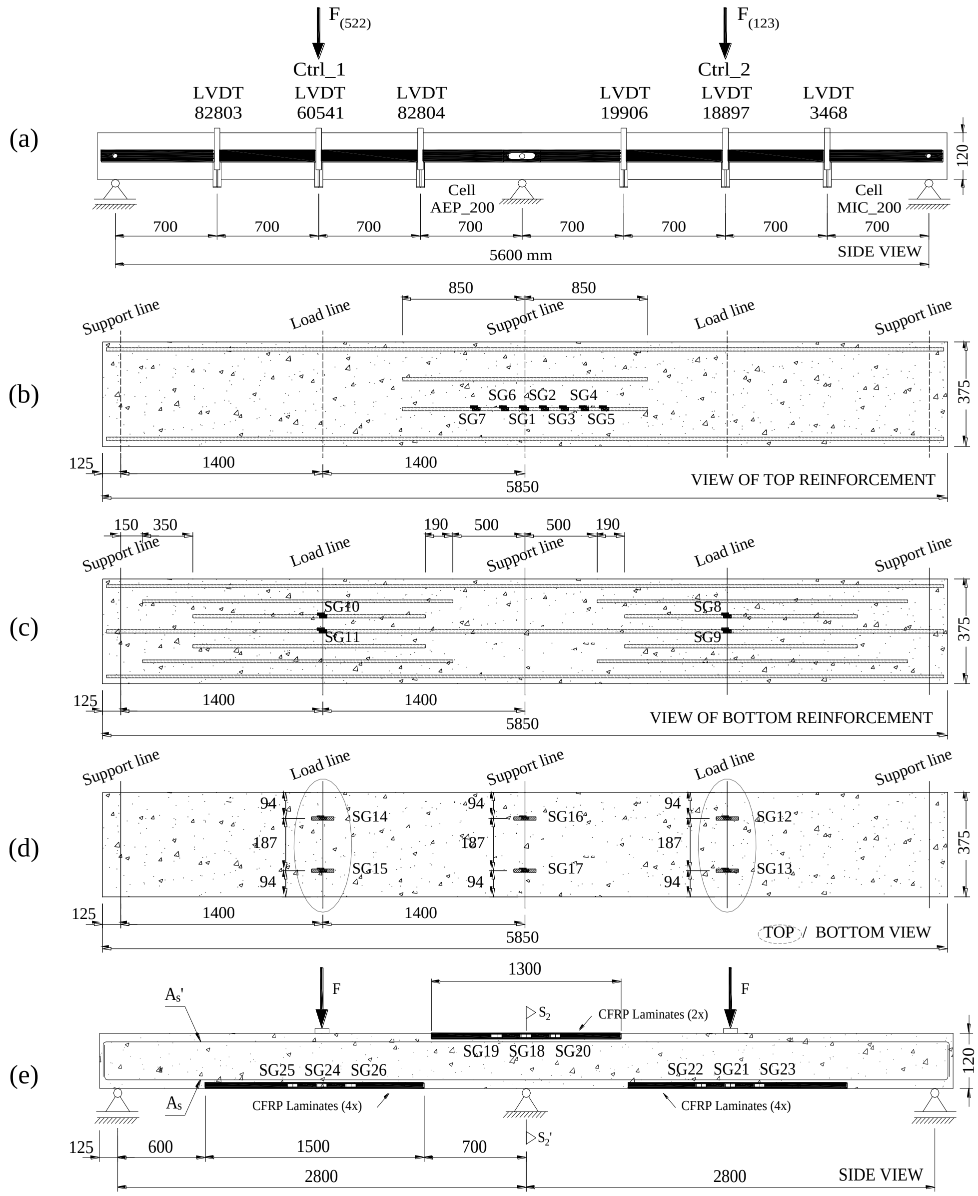

Figure 3 — Arrangement of displacement transducers and strain gauges: (a) displacement transducers; layout of strain gauges at steel bars at hogging (b) and sagging (c) region; (d) strain gauges at concrete slab surfaces, (e) layout of strain gauges at CFRP laminates for SL30s25 (all dimensions are in mm – 1 mm = 0.04 in).

Table 1 — Characteristics of plain concrete.

Slab strip	Property	
	f_{cm} (MPa), [psi]	E_c (GPa), [ksi]
SL30	(30.10), [4365] {1.08}	(31.52), [4570] {0.86}
SL30s25	(32.59), [4726] {1.15}	(30.62), [4441] {2.42}

{value} = Standard deviation

Table 2 — Summary of the properties of steel reinforcement and CFRP laminates.

Steel reinforcement					CFRP Laminate			
Steel bar diameter (ϕs)	Modulus of Elasticity (GPa) [ksi]	Yield stress (0.2 %)[a] (MPa) [psi]	Strain at yield stress[b]	Tensile strength (MPa) [psi]	CFRP laminate height	Ultimate tensile stress (MPa) [ksi]	Ultimate tensile strain (‰)	Modulus of Elasticity (GPa) [ksi]
10 mm (0.39 in.)	(178.24) [25851] {2.48%}	(446.95) [64824] {3.25%}	0.0027 {0.45%}	(575.95) [83534] {0.34%}	10 mm (0.39 in.)	(2867.63) [415914] {3.07%}	17.67 {3.04%}	(159.304) [23105] {3.15%}
12 mm (0.47 in.)	(198.36) [28769] {2.77%}	(442.47) [64174] {2.87%}	0.0024 {0.19%}	(539.88) [78302] {1.84%}	20 mm (0.79 in.)	(2782.86) [403619] {2.73%}	17.76 {3.13%}	(156.69) [22725] {0.73%}

[a]Yield stress determined by the "Offset Method", according to ASTM 370 (2002)
[b]Strain at yield point, for the 0.2 % offset stress
{value} Coefficient of Variation (COV) = (Standard deviation/Average) x 100

Strengthening system

The first step of the NSM strengthening process consisted in opening the slits for the installation of the CFRP laminates, by using a conventional diamond saw cut machine. The slits had a width that varied between 4.5 mm (0.17 in.) and 4.6 mm (0.18 in.) and a depth of 15 mm (0.59 in.) or 27 mm (1.06 in.), depending on the depth of the cross section of the used CFRP laminate, 10 mm (0.39 in.) or 20 mm (0.79 in.), respectively. In order to eliminate the dust resultant from the sawing process, the slits were cleaned using compressed air before bonding the laminates to the concrete into the slits. The CFRP laminates were cleaned with acetone to remove any possible dirt. Finally, the slits were filled with the epoxy adhesive using a spatula, and the CFRP laminates were introduced into the slits.

Main results of the experimental program

The applied loads ($F_{(522)}$ or $F_{(123)}$) versus deflection curves of the tested slab strips are presented in Figures 4 to 6. Additionally, Table 3 presents the main results obtained experimentally. In this Table, $\bar{F}_{\max}$ is the average load ($\bar{F}_{\max} = \left(F_{(522)} + F_{(123)}\right)/2$), $R_{L,\bar{F}_{\max}}$ is the load registered at the load cell (MIC_200) and $\Delta\bar{F}_{\max}/\bar{F}_{\max}^{REF}$ is the increase in terms of load carrying capacity provided by the strengthening technique at $\bar{F}_{\max}$. Figure 6 shows that the adopted NSM strengthening configuration conducted to a significant increase of the load carrying during the second phase of the test loading process. Four phases occurred during each test in the following sequence: a) the uncracked elastic response; b) crack propagation in the hogging and sagging regions with steel bars in elastic stage; c) yielding of the steel reinforcement at the hogging region and crack propagation in the sagging regions with steel bars in elastic stage; d) yielding of the steel reinforcement at the hogging and sagging regions.

As expected, the unstregthened control slab strip behaved in a perfectly plastic manner in the post-yielding phase (after the formation of plastic hinges at hogging and sagging regions), whereas the strengthened slab strips exhibited continuous hardening up to failure. The failure mechanism of the reference slab was governed by flexure failure mode, i.e. by yielding of internal reinforcements, with extensive cracking in the tension flange, followed by concrete crushing in compression parts.

The SL30s25 failed by the detachment of the top concrete cover that includes the laminates in the hogging region (Figure 7 a2). This slab strip had four CFRP laminates mounted in the tension face of the slab over the sagging: two of 1.4x20 mm^2 (0.05 x 0.79 $in.^2$) cross section area and two of 1.4x10 mm^2 (0.05 x 0.39 $in.^2$). Additionally, two CFRP laminates of 1.4x10 mm^2 (0.05 x 0.39 $in.^2$) cross section area were placed in hogging regions. As already mentioned, in the first phase of the test, the strengthened slab strips were loaded up to a deflection of 5.80 mm (0.23 in.), which corresponds to a $\bar{F}$ = 17 kN (3.8 kips). Flexural cracks were first observed at a $\bar{F}$ of about 6 kN (1.3 Kips).

Upon further loading, several flexural cracks formed over the hogging region of both slabs, as shown in Figure 7. The number of flexural cracks has increased with the load, and herringbone cracks formed in the concrete surrounding the CFRP laminates at hogging region.

NUMERICAL SIMULATION

For the prediction of the behaviour of RC continuous slabs strengthened with NSM laminate arrangements capable of increasing the load carrying capacity and assuring high level of moment redistribution for this type of structure, a computer program, based on the finite element method (FEM), was used.

Constitutive laws

According to the present model, a concrete slab is considered a plane shell formulated under the Reissner-Mindlin theory (Barros 1995). In order to simulate the progressive damage induced by concrete cracking and concrete compression nonlinear behavior, the thickness a shell element was discretized in 20 layers that were considered in a state of plane stress.

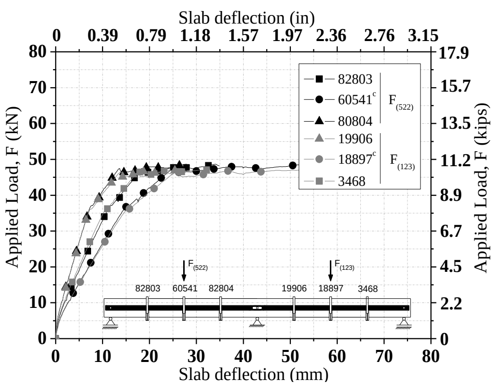

Figure 4 — Load-deflection curves of SL30.

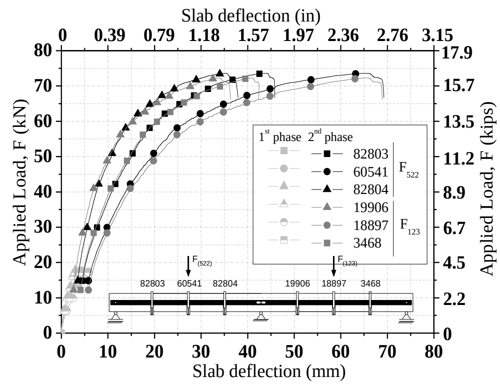

Figure 5 — Load-deflection curves of SL30s25.

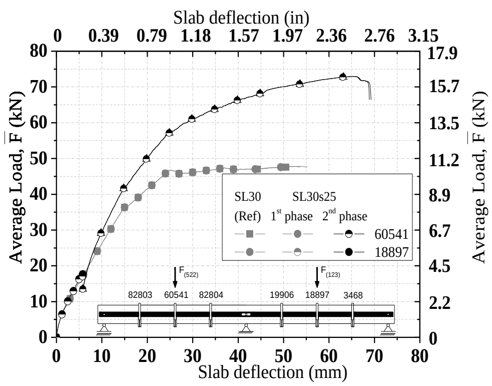

Figure 6 — Load-midspan deflection.

Table 3 — Main results of the experimental program.

Slab strips ID	$\bar{F}_{\max}$, kN (kips)	$R_{L,\bar{F}_{\max}}$, kN (kips)	$\frac{\Delta\bar{F}_{\max}}{\bar{F}_{\max}^{REF}}$ (%)
SL30	47.85 (10.7)	16.43 (3.7)	-----
SL30s25	72.96 (16.4)	26.19 (5.9)	52.47

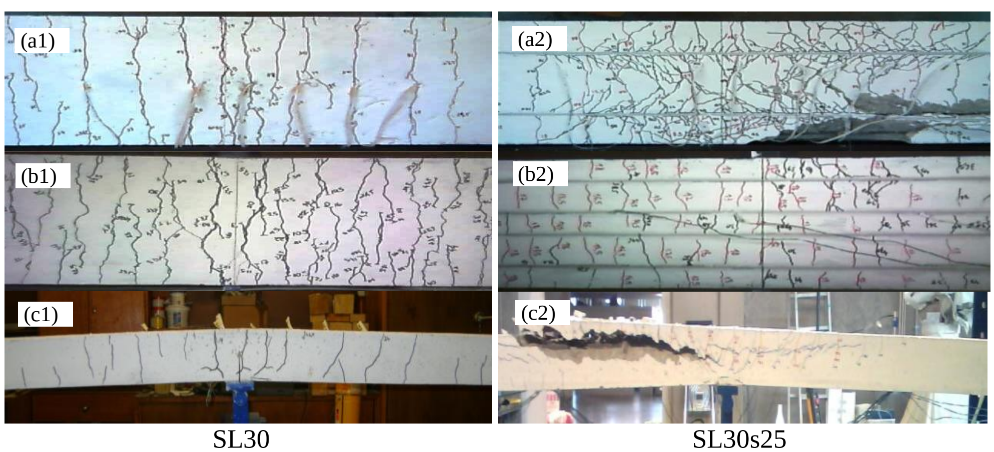

Figure 7 — Crack patterns: plant view at hogging (a1-a2) and sagging regions (b1-b2); lateral view (c1-c2) at hogging region.

The incremental strain vector derived from the incremental nodal displacements obtained under the framework of a nonlinear FEM analysis is decomposed in an incremental crack strain vector, $\Delta\underline{\varepsilon}^{cr}$, and an incremental strain vector of the concrete between cracks, $\Delta\underline{\varepsilon}^{co}$. This last vector is decomposed in an elastic reversible part, $\Delta\underline{\varepsilon}^{e}$, and an irreversible or plastic part, $\Delta\underline{\varepsilon}^{p}$, resulting

$$\Delta\underline{\varepsilon} = \Delta\underline{\varepsilon}^{cr} + \Delta\underline{\varepsilon}^{co} = \Delta\underline{\varepsilon}^{cr} + \Delta\underline{\varepsilon}^{e} + \Delta\underline{\varepsilon}^{p} \tag{1}$$

The incremental stress vector can be computed from the incremental elastic strain vector,

$$\Delta\underline{\sigma} = \underline{D}^{co}\Delta\underline{\varepsilon}^{co} \tag{2}$$

where $\underline{D}^{co}$ is the concrete tangent constitutive matrix,

$$\underline{D}^{co} = \begin{bmatrix} \underline{D}_{mb}^{co} & \phi \\ \phi & \underline{D}_{s}^{co} \end{bmatrix} \tag{3}$$

with $\underline{D}_{mb}^{co}$ and $\underline{D}_{s}^{co}$ being the in-plane and the out-of-plane shear stiffness matrices, respectively. In the present model, concrete behavior is assumed linear elastic in terms of out-of-plane shear. Therefore, the concrete nonlinear behaviour is only considered in the $\underline{D}_{mb}^{co}$ constitutive matrix.

For linear elastic uncracked concrete, $\underline{D}_{mb}^{co}$ is designated by $\underline{D}_{mb}^{eco}$, which is defined elsewhere (Barros and Figueiras 2001). For the case of cracked concrete with concrete between cracks exhibiting an elasto-plastic behavior, $\underline{D}_{mb}^{co}$ of (3) is replaced by $\underline{D}_{mb}^{epcrco}$ (Sena-Cruz *et al*. 2004):

$$\underline{D}_{mb}^{co} \Rightarrow \underline{D}_{mb}^{epcrco} = \underline{D}_{mb}^{epco} - \underline{D}_{mb}^{epco}\left[\underline{T}^{cr}\right]\left(\underline{\hat{D}}^{cr} + \underline{T}^{cr}\,\underline{D}_{mb}^{epco}\left[\underline{T}^{cr}\right]^{T}\right)^{-1}\underline{T}^{cr}\,\underline{D}_{mb}^{epco} \tag{4}$$

where

$$\underline{D}_{mb}^{epco} = \underline{H} - \frac{\underline{H}\dfrac{\partial f}{\partial\underline{\sigma}}\left(\dfrac{\partial f}{\partial\underline{\sigma}}\right)^{T}\underline{H}}{h + \left(\dfrac{\partial f}{\partial\underline{\sigma}}\right)^{T}\underline{H}\left(\dfrac{\partial f}{\partial\underline{\sigma}}\right)} \tag{5}$$

and

$$\underline{H} = \left(\left[\underline{D}_{mb}^{eco}\right]^{-1} + h_{c}\Delta\lambda\frac{\partial^{2} f}{\partial\underline{\sigma}^{2}}\right)^{-1} \tag{6}$$

where $\partial f/\partial\underline{\sigma}$ is the flow vector, h_c is a scalar function that depends on the hydrostatic pressure, $\underline{T}^{cr}$ is a transformation matrix that depends on the direction of the cracks formed at a sampling point (Sena-Cruz *et al*. 2004), and $\underline{\hat{D}}^{cr}$ is the constitutive matrix of the set of cracks. In case of one crack per each sampling point,

$$\underline{\hat{D}}^{cr} = \underline{D}^{cr} = \begin{bmatrix} D_I^{cr} & 0 \\ 0 & D_{II}^{cr} \end{bmatrix} \tag{7}$$

where D_I^{cr} and D_{II}^{cr} are the softening modulus of the fracture modes I and II of the smeared cracks, respectively. D_I^{cr} is characterized by the stress at crack initiation, $\sigma_{n,1}^{cr}$ (see Figure 8), the fracture energy, G_f, the shape of the softening law and the crack band width, l_b.

In smeared crack models the fracture zone is distributed over l_b, which must depend on the finite element geometric characteristics in order to assure that the results of the FEM analysis are not dependent on the finite element mesh (Bazant and Oh 1983). The fracture mode II modulus, D_{II}^{cr}, of (7) is obtained from (Barros 1995):

$$D_{II}^{cr} = \frac{\left(1 - \frac{\varepsilon_n^{cr}}{\varepsilon_{n,u}^{cr}}\right)^{p1}}{1 - \left(1 - \frac{\varepsilon_n^{cr}}{\varepsilon_{n,u}^{cr}}\right)^{p1}} G_c \tag{8}$$

where G_c is the concrete elastic shear modulus and p_1 an integer parameter that can obtain distinct values in order to simulate different levels of concrete shear stiffness degradation (Barros 1995). In case of cracked concrete with concrete between cracks in linear and elastic state, $\underline{D}_{mb}^{co}$ is still obtained from (4) replacing $\underline{D}_{mb}^{epco}$ by $\underline{D}_{mb}^{eco}$.

<u>Steel constitutive law</u>

For modelling the behaviour of the steel bars, the stress-strain relationship represented in Figure 9 was adopted (Sena-Cruz 2004). The curve (under compressive or tensile loading) is defined by the points $PT1 = (\varepsilon_{sy}, \sigma_{sy})$, $PT2 = (\varepsilon_{sh}, \sigma_{sh})$ and $PT3 = (\varepsilon_{su}, \sigma_{su})$, and a parameter p that defines the shape of the last branch of the curve. Unloading and reloading linear branches with slope E_s are assumed in the present approach.

<u>FRP constitutive law</u>

A linear elastic stress-strain relationship was adopted to simulate the behaviour of NSM CFRP laminates applied in the RC slabs.

SIMULATION OF THE TESTS

<u>Materials properties and finite element mesh</u>

Tables 4 and 5 include the values of the parameters adopted for the characterization of the constitutive models for the concrete and steel, respectively.

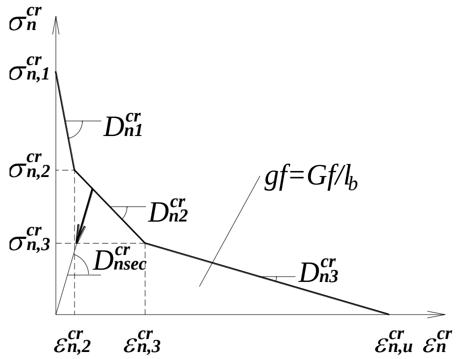

Figure 8 — Tri-linear tensile-softening diagram (Sena-Cruz 2004).

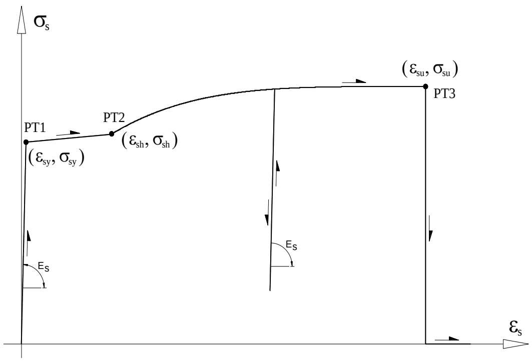

Figure 9 — Uniaxial constitutive model for the steel bars (Sena-Cruz 2004).

The CFRP laminates were assumed as an isotropic material with an elasticity modulus of 156 GPa and null value for the Poisson's coefficient, since the consideration of their real anisotropic properties have marginal influence in terms of their contribution for the behaviour of NSM strengthened RC slabs.

Due to the structural symmetry, only half of the slab was considered in the numerical simulations. Figure 10 shows the eight node finite element mesh adopted to discretize the half part of the slab. The support conditions are also represented in this figure. The slab thickness was discretized in 20 layers.

Results and discussion

Figures 11 to 14 represent relevant results of the simulations corresponding to the slabs of the SL30 series. The figures show that the numerical model is able to capture with good accuracy the behaviour of the constituent materials of this structural system during the loading process of the tested slabs.

Table 6 resumes the results obtained numerically for two scenarios: when a plastic hinge formed at the hogging region (superscript H); when a plastic hinge formed at the sagging regions (superscript S). In this Table, F_y^H and F_y^S are the loads at the formation of the plastic hinge at hogging and sagging regions, respectively, u_y^H and u_y^S are the average deflection for F_y^H and F_y^S, respectively, ε_c^H and ε_c^S are the maximum concrete strains registered at H and S regions, ε_s^H and ε_s^S are the maximum strains in steel bars at H and S regions, respectively, and, finally, ε_f^H and ε_f^S are the maximum strains in the CFRP laminates at H and S regions.

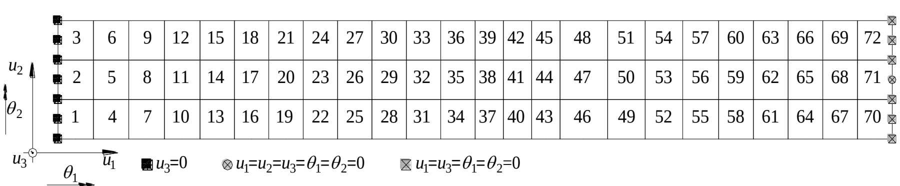

Figure 10 — Finite element mesh adopted to discretize the half part of a RC slab.

Table 4 — Values of the parameters of the concrete constitutive model.

Poisson´s ratio (ν_c)	0.15
Initial Young´s modulus (E_c)	29.83 GPa (4326 ksi)
Compressive strength (f_c)	28.40 MPa (4119 psi)
Strain at peak compression stress	$\varepsilon_{c,1}$ = 1.98×10^{-3}
Parameter defining the initial yield surface (Sena-Cruz 2004)	α_0 = 0.4
Tri-linear tension softening/stiffening diagram(1)	f_{ct} = 1.50 MPa (217 psi) G_f = 0.052 N/mm (0.30 lb/in.) ξ_1 = 0.015; α_1 = 0.6 ξ_2 = 0.2; α_2 = 0.25
Parameter defining the mode I fracture energy available to the new crack (Barros 1995)	n = 2
Shear retention factor (p_1 factor of Equation (8))	p_1 = 2
Crack band-width	Square root of the area of Gauss integration point
Threshold angle (Barros 1995)	α_{th} = 30º
Maximum number of cracks per integration point	2

(1) $f_{ct} = \sigma^{cr}_{n,1}$; $\xi_1 = \varepsilon^{cr}_{n,2} / \varepsilon^{cr}_{n,u}$; $\alpha_1 = \sigma^{cr}_{n,2} / \sigma^{cr}_{n,1}$; $\xi_2 = \varepsilon^{cr}_{n,3} / \varepsilon^{cr}_{n,u}$; $\alpha_2 = \sigma^{cr}_{n,3} / \sigma^{cr}_{n,1}$ (see Figure 8)

Table 5 — Values of the parameters of the steel constitutive model (see Figure 9).

Steel bar diameter	PT1 $\begin{pmatrix} \varepsilon_{sy}[-] \\ \sigma_{sy}(MPa),[psi] \end{pmatrix}$	PT2 $\begin{pmatrix} \varepsilon_{sh}[-] \\ \sigma_{sh}(MPa),[psi] \end{pmatrix}$	PT3 $\begin{pmatrix} \varepsilon_{su}[-] \\ \sigma_{su}(MPa),[psi] \end{pmatrix}$	E_s (GPa) [ksi]
8 mm (0.31 in.)	2.50×10^{-3} (421.00), [61060]	4.42×10^{-2} (526.25), [76326]	8.85×10^{-2} (555.72), [80600]	(200.80) [29123]
10 mm (0.39 in.)	2.50×10^{-3} (446.00), [64686]	3.07×10^{-2} (446.00), [64686]	1.31×10^{-1} (557.50), [80858]	(178.24) [25851]
12 mm (0.47 in.)	2.50×10^{-3} (445.00), [64541]	3.05×10^{-2} (445.00), [64541]	1.02×10^{-1} (547.35), [79386]	(198.36) [28769]

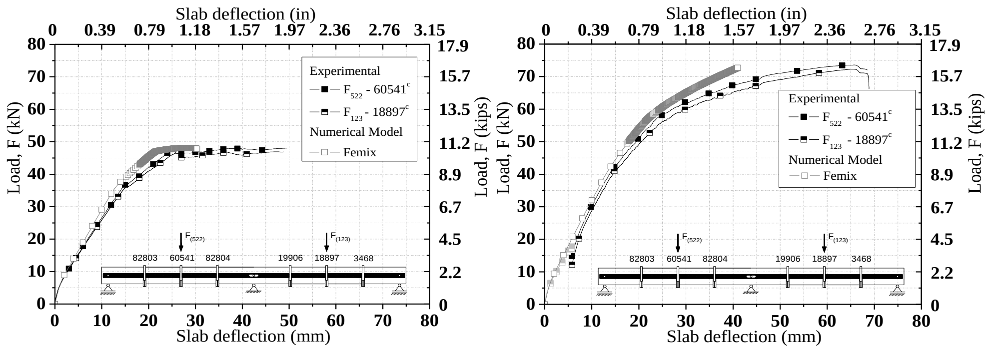

(a) (b)

Figure 11 — Force-loaded section deflection relationship: (a) SL30 and (b) SL30s25.

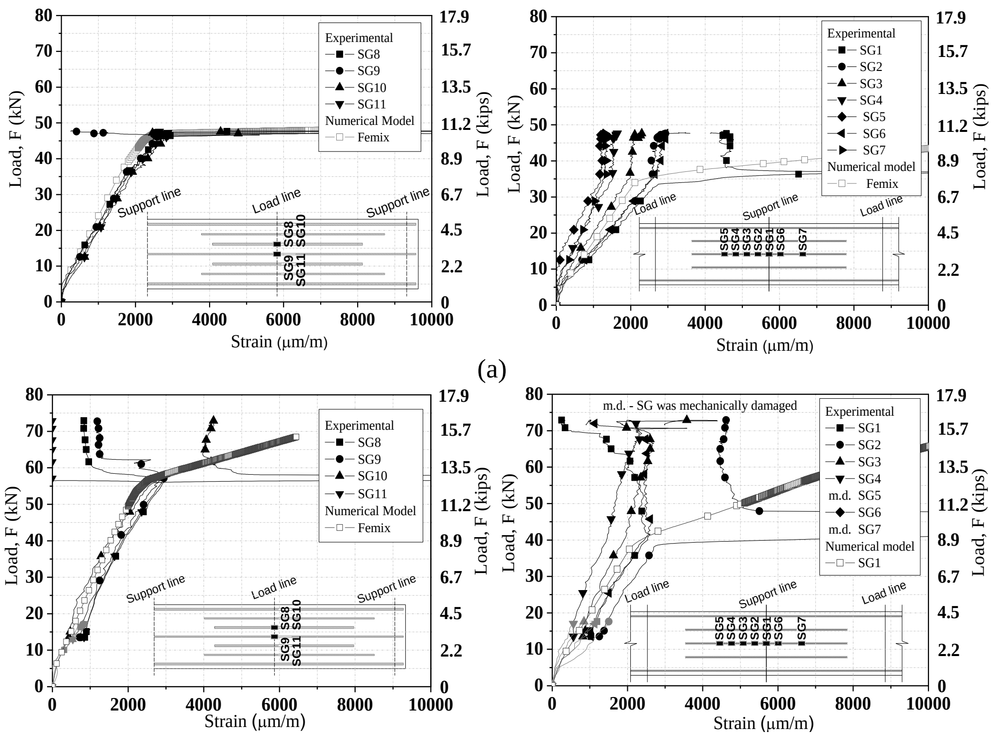

(a)

(b)

Figure 12 — Force –strain relationships in steel: (a) SL30 and (b) SL30s25.

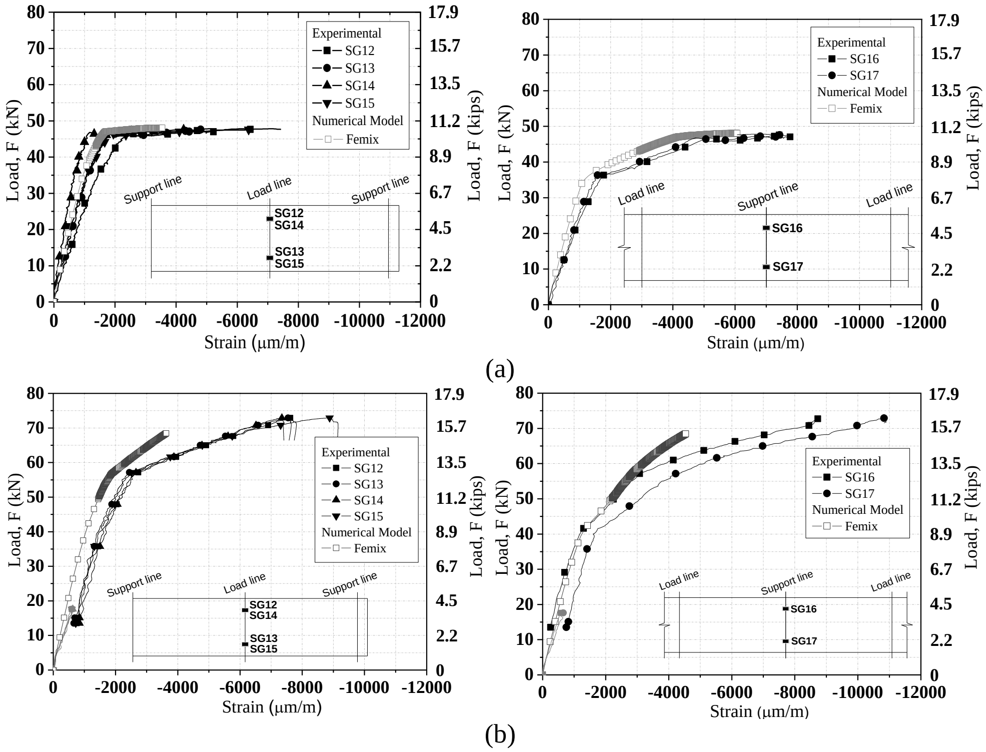

Figure 13 — Force –strain relationships in concrete: (a) SL30 and (b) SL30s25.

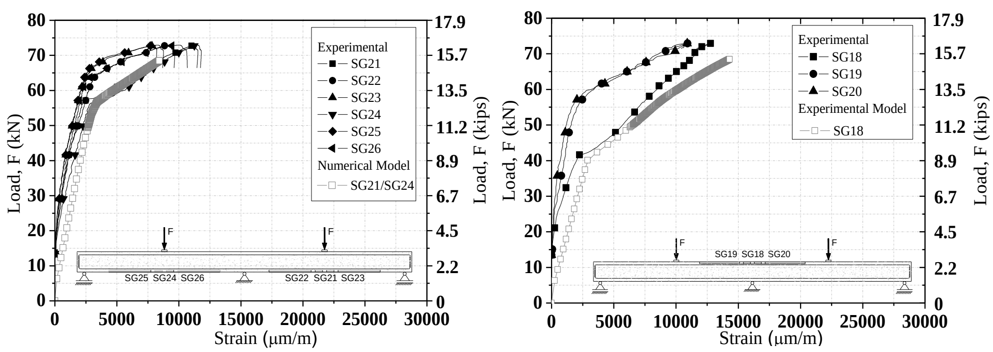

Figure 14 — Force –strain relationships in CFRP laminates of SL30s25.

Table 7 presents the relevant results when the maximum concrete compressive strain attained 3.5 ‰ (symbols with subscript "*cu*") in the hogging and sagging regions ($\varepsilon_{c,\max} = 3.5‰$, which is assumed the concrete crushing strain).

In this Table, IR represents the increase in terms of load carrying capacity provided by the strengthening technique, calculated according to the following equation:

Table 6 — Numerical results at the formation of the hinges

Hinge at hogging region (H)			Hinge at sagging region (S)		
Slab strip ID	SL30	SL30s25	Slab strip ID	SL30	SL30s25
F_y^H (kN) [kips]	(36.23) [8.1]	(40.12) [9.0]	F_y^S (kN) [kips]	(45.16) [10.2]	(53.72) [12.1]
u_y^H (mm) [in]	(13.00) [0.51]	(13.00) [0.51]	u_y^S (mm) [in]	(19.79) [0.78]	(19.88) [0.78]
ε_c^H (‰)	-1.21	-1.23	ε_c^H (‰)	-3.51	-2.52
ε_c^S (‰)	-1.00	-1.05	ε_c^S (‰)	-1.50	-1.66
ε_s^S (‰)	1.60	1.54	ε_s^S (‰)	2.23	2.23
ε_s^H (‰)	2.40	2.30	ε_s^H (‰)	11.94	6.05
ε_f^H (‰)	------	2.90	ε_f^H (‰)	------	7.74
ε_f^S (‰)	------	2.05	ε_f^S (‰)	------	3.00

Table 7 — Experimental results at concrete crushing

Concrete crushing initiation at hogging region ($\varepsilon_{cu}^H = 3.5‰$)			Concrete crushing initiation at sagging regions ($\varepsilon_{cu}^S = 3.5‰$)		
Slab strip ID	SL30	SL30s25	Slab strip ID	SL30	SL30s25
F_{cu}^H (kN) [kips]	(45.15) [10.1]	(62.34) [14.0]	F_{cu}^S (kN) [kips]	(48.04) [10.8]	(67.67) [15.2]
u_{cu}^H (mm) [in]	(19.77) [0.78]	(26.83) [1.06]	u_{cu}^S (mm) [in]	(27.10) [1.07]	(33.48) [1.32]
$\varepsilon_{c,\max}^S$ (‰)	-1.50	-2.67	$\varepsilon_{c,\max}^H$ (‰)	-6.01	-4.39
$\varepsilon_{s,\max}^S$ (‰)	2.23	4.37	$\varepsilon_{s,\max}^S$ (‰)	8.81	6.17
$\varepsilon_{s,\max}^H$ (‰)	11.93	8.75	$\varepsilon_{s,\max}^H$ (‰)	20.54	10.85
$\varepsilon_{f,\max}^H$ (‰)	------	11.17	$\varepsilon_{f,\max}^H$ (‰)	------	13.86
$\varepsilon_{f,\max}^S$ (‰)	------	5.76	$\varepsilon_{f,\max}^S$ (‰)	------	8.07
η (%)	22.75	18.82	η (%)	26.88	19.37
IR (%)		38.07	IR (%)		40.86

$$IR = \frac{F_{cu}^{CFRP} - F_{cu}^{REF}}{F_{cu}^{CFRP}} 100 \qquad (9)$$

where F_{cu}^{CFRP} and F_{cu}^{REF} are the load of the strengthened and reference slabs, respectively. From the analysis of the results included in Tables 6 and 7 and represented in Figures 11 to 14 it can be outlined the following:

- after crack initiation, which occurred for a load of about 6 kN (1.3 kips), the slab stiffness decreased significantly, but the elasto-cracked stiffness was almost maintained up to the formation of the plastic hinge at the intermediate support, at a load level of about 36 kN (8.1 kips) and 40 kN (8.9 kips) for the reference and SL30s25 slabs, respectively.
- For a compressive strain of 3.5 ‰, the increase of the load carrying capacity provided by the strengthening system was of about 39 %. This value reveals that the aimed increase in terms of slab's load carrying capacity was attained.
- Up to the formation of the plastic hinges the strains in the laminates ranged from 2.05‰ to 7.74‰, which justifies the relative low contribution of the laminates for the load carrying capacity up to this load level. In fact, the force-deflection relationship evinces that, up to the formation of the plastic hinge at the intermediate support, CFRP strips did not contribute significantly for the slabs' load carrying capacity. However, at concrete crushing at the sagging regions, the maximum strain in the CFRP laminates varied between 8.07‰ and 13.86‰, which is 45 to 78 % of the CFRP laminate ultimate strain.
- The deflection at F_y^S, u_y^S, was not significantly affected by the presence of the CFRP laminates.
- The contribution of the CFRP laminates for the slab's maximum load carrying capacity was limited due to the occurrence of concrete crushing, and the premature failure mode by the detachment of the concrete cover layer that includes the laminates at the hogging region.

MOMENT REDISTRIBUTION ANALYSIS

The percentages of moment redistribution obtained numerically for the slab strips are shown in Figure 15. The SL30 slab strip exhibited a moment redistribution rate of about 8.84 % at the yielding of steel reinforcement at the central support section. At the yielding of reinforcement at the sagging region, the moment redistribution increased to about 22.76 %. For a compressive strain of 3.5 ‰ at H and S moment redistribution rates of about 22.74% and 26.88% were obtained, respectively.

Concerning to SL30s25 slab strip, a moment redistribution of 8.49 % was obtained when the steel reinforcement yields at the hogging region. Afterwards, a moment redistribution of 15.76 % was obtained at the yielding of steel reinforcement at the sagging region. Finally, for a compressive strain of 3.5 ‰ at H and S, respectively, moment redistribution rates of about 18.22% and 19.37% were obtained. Figure 16 shows the variation of the negative (M^-) and positive (M^+) moments with the increase of the applied load. The tendency of the M-F relationship to approximate to the elastic relationship when a 30% of moment redistribution was assumed indicates that the moment redistribution mechanism was formed.

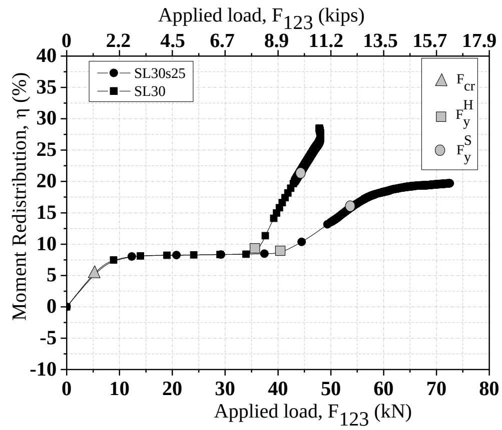

Figure 15 — Moment redistribution-applied load relationship obtained numerically for the slabs.

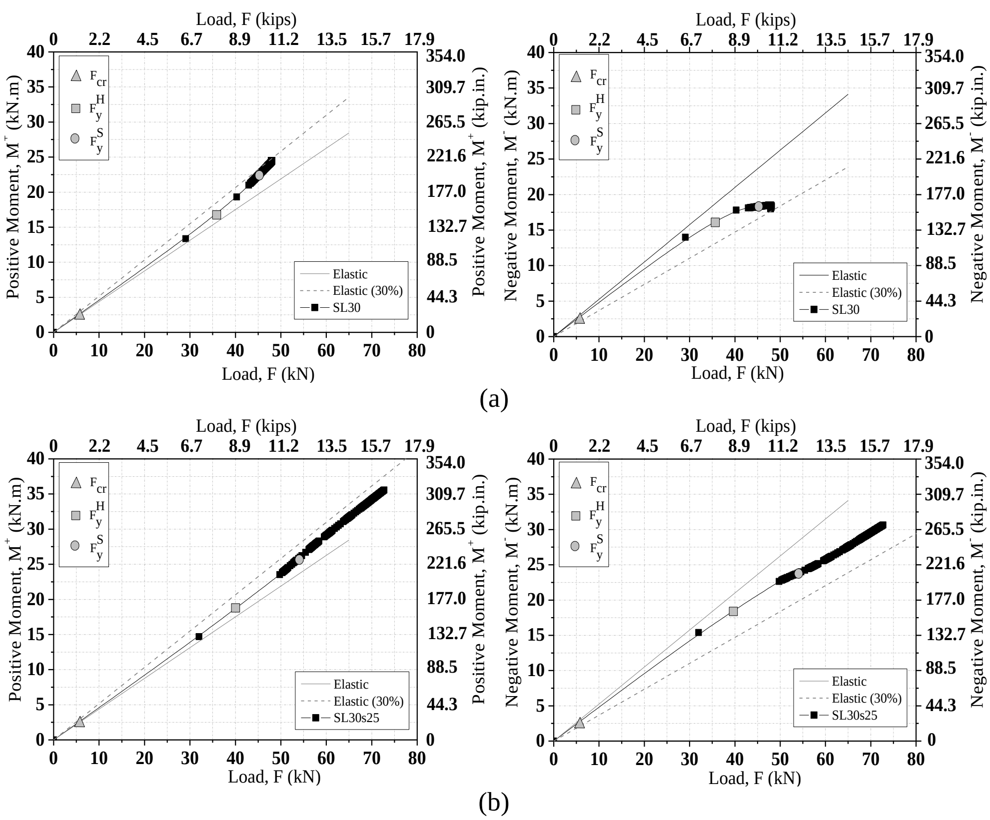

Figure 16 — Bending moment -applied load relationship: (a) SL30 and (b) SL30s25.

CONCLUSIONS

This work deals with the use of the near surface mounted (NSM) CFRP laminates for the flexural strengthening of continuous reinforced concrete (RC) slabs not only in terms of load carrying capacity, but also in the context of moment redistribution capacity. The strengthening procedures adopted in the laboratory tests followed, as much as possible, the real strengthening practice for this type of interventions.

The obtained results show that the proposed technique is able to increase the load carrying capacity of RC slabs and preserves relevant levels of moment redistribution. However, the load carrying capacity of the strengthened slab was limited by the detachment of the strengthened concrete cover layer at the intermediate support.

For validation purposes, a computer program, based on the finite element method (FEM), was used. Using the obtained experimental results, the capability of the FEM-based computer program to predict with high accuracy the behaviour of this type of structures up to its collapse was highlighted.

ACKNOWLEDGEMENTS

The authors wish to acknowledge the support provided by the “Empreiteiros Casais”, S&P®, Secil (Unibetão, Braga) Companies. The study reported in this paper forms a part of the research program “CUTINEMO - Carbon fiber laminates applied according to the near surface mounted technique to increase the flexural resistance to negative moments of continuous reinforced concrete structures” supported by FCT, PTDC/ECM/73099/2006. The first author would like to acknowledge the National Council for Scientific and Technological Development (CNPq) – Brazil for financial support for scholarship (GDE 200953/2007-9).

REFERENCES

ACI Committee 318, “Building code requirements for structural concrete and Commentary (ACI 318-04)”, Reported by committee 318, American Concrete Institute, Detroit, 351 pp., 2004.

ACI Committee 440, “Guide for the design and construction of externally bonded FRP systems for strengthening concrete structures”, American Concrete Institute, 118 p, 2007.

Akbarzadeh Bengar, H., Maghsoudi, A.A., “Experimental investigations and verification of debonding strain of RHSC continuous beams strengthened in flexure with externally bonded FRPs”, Materials and Structures Journal, 10.1617/s11527-009-9550-7, September 2009.

Anwarul Islam, A.K.M., “Effective methods of using CFRP bars in shear strengthening of concrete girders”, Engineering Structures, 31(3), 709-714, March 2009.

Ashour, A. F., El-Refaie, S.A. and Garrity, S.W., ”Flexural strengthening of RC continuous beams using CFRP laminates”, Cement & Concrete Composites, 26 (2004), 765 – 775, 2004.

ASTM 370, “Standard test methods and definitions for mechanical testing of steel products”, American Society for Testing and Materials, 2002.

Barros, J.A.O., “Comportamento do betão reforçado com fibras - análise experimental e simulação numérica (Behavior of FRC – experimental analysis and numerical simulation)”, PhD Thesis, Civil Eng. Dept., Faculty of Engineering, University of Porto, Portugal, 1995 (in Portuguese).

Barros, J.A.O.; Figueiras, J.A., “Nonlinear analysis of steel fibre reinforced concrete slabs on grade”, Computers & Structures Journal, Vol.79, No.1, pp. 97-106, January 2001.

Barros, J.A.O., Fortes, A.S., “Flexural strengthening of concrete beams with CFRP laminates bonded into slits”, Journal Cement and Concrete Composites, 27(4), 471-480, 2005.

Barros, J.A.O., Dias, S.J.E., “Near surface mounted CFRP laminates for shear strengthening of concrete beams”, Cement & Concrete Composites 28, 276–292, 2006.

Barros, J.A.O., Dias, S.J.E., Lima, J.L.T, “Efficacy of CFRP-based techniques for the flexural and shear strengthening of concrete beams”, Journal Cement and Concrete Composites, 29(3), 203-217, March 2007.

Barros, J.A.O., Kotynia, R., “Possibilities and challenges of NSM for the flexural strengthening of RC structures”, Fourth International Conference on FRP Composites in Civil Engineering (CICE2008), Zurich, Switzerland, 22-24July 2008.

Bazant, Z.P., Oh, B.H., Crack band theory for fracture of concrete. Materials and Structures, RILEM, 1983, 16(93), 155-177.

Bonaldo, E., “Composite materials and discrete steel fibres for the strengthening of thin concrete structures”, PhD Thesis, University of Minho, Guimarães, Portugal, 2008.

Carolin, A., “Carbon fibre reinforced polymers for strengthening of structural elements”, Doctoral Thesis, Lulea Univ. of Technology, Lulea, Sweden, 2003.

CEB-FIP Model Code 1990. (1993). “Design Code”. Thomas Telford, Lausanne, Switzerland.

De Lorenzis, L., A. Nanni, and A. La Tegola, "Strengthening of Reinforced Concrete Structures with Near Surface Mounted FRP Rods" , bibl. International Meeting on Composite Materials, PLAST 2000, Milan, Italy, May 9-11, 2000.

Dias, S.J.E., Barros, J.A.O., “Shear strengthening of T cross section reinforced concrete beams by near surface mounted technique”, Journal Composites for Construction, 12(3), 300-311, May/June 2008.

Dias, S.J.E.; Barros, J.A.O., “Performance of reinforced concrete T beams strengthened in shear with NSM CFRP laminates”, Engineering Structures, 32(2), 373-384, February 2010

El-Hacha, R., Rizkalla, S.H., “Near-surface-mounted fiber-reinforced polymer reinforcements for flexural strengthening of concrete structures”, ACI Structural Journal, 101(5), 717-726, 2004.

El-Refaie, S. A., Ashour, A. F. and Garrity, S. W., “Sagging and hogging strengthening of continuous reinforced concrete beams using CFRP sheets”, ACI Structural Journal, 100(4), 446-453, July-August 2003.

FIB - Bulletin 14, “Externally bonded FRP reinforcement for RC structures”, Technical report by Task Group 9.3 FRP, 130 p, 2001.

Grace, N.F., Ragheb, W.F. and Abdel-Sayed, G., “Strengthening of Cantilever and Continuous Beams using New Triaxially Braided Ductile Fabric.” ACI Structural Journal, 101, 237-244, 2004.

ISO 527-1, “Plastics - Determination of tensile properties - Part 1: General principles”, International Organization for Standardization (ISO), Genèva, Switzerland, 9 pp, 1993.

ISO 527-2, “Plastics - Determination of Tensile Properties - Part 2: Test Conditions for Moulding and Extrusion Plastics”, International Organization for Standardization (ISO), Geneva, Switzerland, 1993.

ISO 527-5, “Plastics - Determination of tensile properties - Part 5: Test conditions for unidirectional fibre-reinforced plastic composites”, International Organization for Standardization (ISO), Genèva, Switzerland, 9 pp, 1993.

LNEC E397 (1993) Concrete—Assessment of the elasticity modulus under uniaxial compression. Laboratório Nacional de Engenharia Civil, (in Portuguese).

Liu, I.S.T., “Intermediate crack debonding of plated reinforced concrete beams”, PhD Thesis, School of Civil and Environmental Engineering, The University of Adelaide, Adelaide, Australia, November 2005.

Liu, I.S.T., Oehlers, D.J. and Seracino, R., “Tests on the ductility of reinforced concrete beams retrofitted with FRP and steel near-surface mounted plates”, Journal of Composites for Construction, 10(2), 106-114, 2006.

Nordin, H., “Flexural strengthening of concrete structures with prestressed near surface mounted CFRP rods”, Licentiate Thesis, Lulea Univ. of Technology, Lulea, Sweden, 2003.

Sena-Cruz, J.M.; Barros, J.A.O.; Azevedo, A.F.M., "Elasto-plastic multi-fixed smeared crack model for concrete", Technical report 04-DEC/E-05, Dep. Civil Eng., University of Minho, 70 pp, June 2004.

Sena-Cruz, J.M. “Strengthening of concrete structures with near-surface mounted CFRP laminate strips.” PhD Thesis, Department of Civil Engineering, University of Minho, (2004).

Vasseur, L., “Non linear behavior of continuous concrete beams strengthened with Externally Bonded FRP Reinforcement”, Doctoral Thesis, Ghent University, Ghent, Belgium, 2009.